Fundamental Two-Stage Formulation for Bayesian System Identification, Part II: Application to Ambient Vibration Data

Feng-Liang Zhang[1*] and Siu-Kui Au[2]

[1] Research Institute of Structural Engineering and Disaster Reduction, Tongji University, China

[2] Center for Engineering Dynamics and Institute for Risk and Uncertainty, University of Liverpool, UK

Abstract

A fundamental theory has been developed for a general two-stage Bayesian system identification problem in the companion paper (Part I). This paper applies the theory to the particular case of structural system identification using ambient vibration data. In Stage I, the modal properties are identified using Fast Bayesian FFT method. Given the data, their posterior distribution can be well approximated by a Gaussian distribution whose mean and covariance matrix can be computed efficiently. In Stage II, the structural model parameters (e.g., stiffness, mass) are identified incorporating the posterior distribution of the natural frequencies and mode shapes in Stage I and their conditional distribution based on the theoretical structural finite element model. Synthetic and experimental data are used to illustrate the proposed theory and applications. A number of factors commonly relevant to structural system identification are studied, including the number of measured degrees of freedom, the number of identifiable modes and sensor alignment error.

Keywords:

Ambient modal identification; Bayesian operational modal analysis; system identification; two-stage approach; Fast Bayesian FFT method

[*] Corresponding author. E-mail: fengliangzhang@hotmail.com, fengliangzhang@tongji.edu.cn; Office phone: +86 21 6598 7352; Office fax: +86 21 6598 2668

1 Introduction

A general theory has been presented in the companion paper [1] for a two-stage Bayesian system identification problem. It fundamentally expresses the posterior probability density function (PDF) of structural model parameters in Stage II in terms of the posterior PDF of the modal parameters in Stage I. In this paper, the theory is applied to the identification of structural model parameters (e.g., stiffness, mass), which is the problem originally motivated the development of the general theory. The data is assumed to consist of digital acceleration time histories measured at a limited number of degrees of freedom (dofs) of the subject structure under ambient environment. The loading is unknown but assumed to be broadband random within the resonance band of the identified modes. This context is of high relevance in practice, as ambient vibration tests are becoming economically viable and commercially sustainable [2][3]. It is also of high scientific relevance because the identification uncertainty of modal parameters based on (output-only) ambient data is often significantly higher than their counterparts identified from properly managed free or forced vibration data. As mentioned in the companion paper, different variants of two-stage Bayesian formulations for structural system identification have been proposed, e.g., [4][5][6][7][8][9], although they all involve heuristics in the formulation of the likelihood function in Stage II.

For clarity we first give an overview of the two-stage approach applied to structural identification problem in the context of the theoretical framework developed in the companion paper. Using ambient vibration data, the objective is to identify the set of structural model parameters $\boldsymbol{\theta}$ involved in the characterization of the finite element model of the real structure, e.g., stiffness, mass, boundary conditions, etc. In Stage I, Fast Bayesian FFT (Fast Fourier Transform) method is used for identifying the modal properties based on ambient vibration data [10][11][12][13]; see a recent review in [14]. The method is well-suited for ambient modal identification for its computational efficiency and assumption robustness. Operating in the frequency domain, the data D effectively consists of the FFT of the measured acceleration time histories within the resonance frequency bands of the modes selected by the analyst. As far as structural

system identification is concerned, the information content of this FFT data is equivalent to the original time domain data, because the FFTs in other frequency bands are irrelevant or difficult to model. Using only the FFT data in the selected frequency bands for identification significantly reduces the number of modal parameters to be identified simultaneously and requires minimal assumption on the ambient excitation.

The full set of modal parameters $\boldsymbol{\alpha}$, from which an explicit likelihood function $p(D|\boldsymbol{\alpha})$ can be derived, comprises the natural frequencies, damping ratios, partial mode shapes (i.e., confined to the measured dofs), the power spectral density (PSD) matrix of the modal forces and the PSD of the prediction error (arising from, e.g., sensor noise). With sufficient data, these parameters are globally identifiable and their posterior PDF can be well approximated by a Gaussian distribution with mean and covariance matrix that can be computed efficiently. Uniform (i.e., constant) prior distributions are used in practice for modal identification problems. As a result, the hypothetical posterior PDF $p_0(\boldsymbol{\alpha}|D)$ and the actual posterior PDF $p(\boldsymbol{\alpha}|D)$ are identical. Within $\boldsymbol{\alpha}=[\varpi,\boldsymbol{\upsilon}]$, the set ϖ for identifying the structural parameters in Stage II comprises the natural frequencies and partial mode shapes because they can be theoretically predicted by a structural (e.g., finite element) model. The set $\boldsymbol{\upsilon}$ comprises the remaining modal parameters, i.e., the damping ratios, PSD matrix of modal forces and the PSD of prediction error. As a property of Gaussian distribution, the marginal distribution $p_0(\varpi|D)$ is also Gaussian, whose mean and covariance matrix can be directly taken from those of the full distribution $p_0(\boldsymbol{\alpha}|D)$.

This work focuses on the case when there is no structural prediction error. That is, the natural frequencies and mode shapes can be completely determined by the structural parameters so that $p(\varpi|\boldsymbol{\theta})=\delta(\varpi-\tilde{\varpi}(\boldsymbol{\theta}))$ is a Dirac-Delta function centered at the theoretical structural model prediction $\tilde{\varpi}(\boldsymbol{\theta})$. This scope is considered as it is consistent with the conventional scenario studied in the literature, providing a starting point for applying the general theory. Modeling $p(\varpi|\boldsymbol{\theta})$ in a non-trivial manner and incorporating its information for updating $\boldsymbol{\theta}$ requires substantially more consideration that deserves a separate line of research.

This paper is organized as follows. The structural modeling assumptions are first described, followed by an outline of Fast Bayesian FFT method in Stage I. Theoretical and computational issues in Stage II are discussed. A comparison with the conventional formulations is then given, followed by a summary of the whole procedure. Illustrative examples with synthetic and experimental data are presented to verify the method with applications.

2 Problem context

Consider a linear elastic structure, modeled by the conventional structural dynamics equation

$$\mathbf{M}\ddot{\mathbf{x}}(t)+\mathbf{C}\dot{\mathbf{x}}(t)+\mathbf{K}\mathbf{x}(t)=\mathbf{W}(t) \tag{1}$$

where $\mathbf{M}$, $\mathbf{C}$, $\mathbf{K}$, $\mathbf{W}$ are the mass matrix, damping matrix, stiffness matrix and force vector, respectively. Assuming classical damping, the response can be expressed as a sum of modal contributions:

$$\mathbf{x}(t)=\sum_i \mathbf{u}_i \eta_i(t) \tag{2}$$

where $\mathbf{u}_i$ and η_i are respectively the full mode shape and modal response of the i-th mode; the sum is overall all modes of the structure. The full mode shape $\mathbf{u}_i$ satisfies the generalized eigenvalue equation:

$$\mathbf{K}\mathbf{u}_i=\omega_i^2\mathbf{M}\mathbf{u}_i \tag{3}$$

where $\omega_i=2\pi f_i$ and f_i are the natural frequency in rad/sec and in Hz, respectively. The modal response η_i satisfies the uncoupled modal equation of motion:

$$\ddot{\eta}_i(t)+2\zeta_i\omega_i\dot{\eta}_i(t)+\omega_i^2\eta_i(t)=w_i(t) \tag{4}$$

where

$$w_i(t)=\frac{\mathbf{u}^T\mathbf{W}(t)}{\mathbf{u}^T\mathbf{M}\mathbf{u}} \tag{5}$$

is the modal force.

The goal of the structural identification problem in this paper is to identify the structural parameters $\boldsymbol{\theta}$ from ambient vibration data of the as-built structure at a limited number of dofs. Only the stiffness matrix $\mathbf{K}$ and the mass matrix $\mathbf{M}$ are assumed to possibly depend on $\boldsymbol{\theta}$. This assumption arises from practical consideration in structural engineering where there is no acceptable means for modeling the damping of real structures. The loading $\mathbf{W}(t)$ is not measured but is assumed to be broadband random in the specific sense that the modal force $w_i(t)$ of the identified modes has a constant PSD within resonance frequency bands selected by the analyst.

Let $\{\hat{\mathbf{y}}_j \in R^n : j = 1,..., N\}$, abbreviated as $\{\hat{\mathbf{y}}_j\}$, denote the time domain acceleration data at n measured degrees of freedom (dofs) of the structure; N is the number of data points. The FFT $\{\hat{F}_k\}$ of $\{\hat{\mathbf{y}}_j\}$ is defined as

$$\hat{F}_k = \sqrt{\frac{2\Delta t}{N}} \sum_{j=1}^{N} \hat{\mathbf{y}}_j \exp[-2\pi \mathbf{i} \frac{(j-1)(k-1)}{N}] \tag{6}$$

where $\mathbf{i}^2 = -1$; $\hat{F}_k$ corresponds to frequency abscissa $\mathrm{f}_k = (k-1)/N\Delta t$ for $k = 1,..., N_q$; Δt is the sampling interval; N_q is the index corresponding to the Nyquist frequency, equal to the integer part of $1 + N/2$. Operating in the frequency domain, the data D used for system identification effectively consists of the FFT within a number of disjoint frequency bands containing the modes that can be identified, i.e.,

$$D = \{D^{(r)} : r = 1,..., n_B\} \tag{7}$$

where $D^{(r)}$ denotes the collection of FFT $\{\hat{F}_k\}$ in the r-th frequency band.

In Stage I, the set of modal parameters that completely defines the distribution of D is given by

$$\boldsymbol{\alpha} = [\varpi, \upsilon] \tag{8}$$

Here ϖ comprises the natural frequencies and partial mode shapes (i.e., confined to the measured dofs)

$$\varpi = \{\mathbf{f}, \boldsymbol{\Phi}\} \tag{9}$$

where $\mathbf{f}$ and $\mathbf{\Phi}$ denote respectively the collection of all natural frequencies and mode shapes within all the selected bands. On the other hand, $\boldsymbol{\upsilon}$ consists of the remaining modal parameters

$$\boldsymbol{\upsilon} = \{\boldsymbol{\zeta}, \mathbf{S}, \mathbf{S}_e\} \tag{10}$$

where $\boldsymbol{\zeta}$, $\mathbf{S}$ and $\mathbf{S}_e$ denote respectively the collection of the damping ratios, PSD of modal forces and PSD of prediction errors in all selected frequency bands.

With little loss of generality, a uniform (constant) prior distribution is assumed for the modal parameters $\boldsymbol{\upsilon} = [\boldsymbol{\zeta}, \mathbf{S}, \mathbf{S}_e]$ that are not related to the structural parameters $\boldsymbol{\theta}$. This is justified because for sufficient data often encountered in practice the likelihood function in the modal identification problem is fast varying compared to the prior distribution. On the other hand, the prior distribution for $\varpi = [\mathbf{f}, \mathbf{\Phi}]$ is not subjected to free choice because it is already determined by $p(\boldsymbol{\theta})$ and the conditional distribution $p(\varpi \mid \boldsymbol{\theta})$ (structural prediction model) through

$$p(\varpi) = \int p(\varpi \mid \boldsymbol{\theta}) p(\boldsymbol{\theta}) d\boldsymbol{\theta} \tag{11}$$

Nevertheless, according to the standard formulation, this PDF is immaterial as it is not involved in the computations.

In the next two sections we shall discuss the formulation of the (hypothetical) posterior distribution $p_0(\varpi \mid D)$ in Stage I and the conditional distribution $p(\varpi \mid \boldsymbol{\theta})$ that connects Stage I and II. These allow the posterior distribution $p(\boldsymbol{\theta} \mid D)$ to be obtained in Stage II according to (29) in the companion paper:

$$p(\boldsymbol{\theta} \mid D) \propto p(\boldsymbol{\theta}) \int p_0(\varpi \mid D) p(\varpi \mid \boldsymbol{\theta}) d\varpi \tag{12}$$

3 Modal identification (Stage I)

In Stage I, the modal parameters $\boldsymbol{\alpha} = \{\mathbf{f}, \boldsymbol{\xi}, \mathbf{\Phi}, \mathbf{S}, \mathbf{S}_e\}$ are identified from the data D, i.e., FFT within the resonance frequency bands of modes selected by the analyst. Although only the identification result of $\varpi = \{\mathbf{f}, \mathbf{\Phi}\}$ is used in Stage II through $p_0(\varpi \mid D)$, the full

set of modal parameters $\boldsymbol{\alpha} = [\boldsymbol{\varpi}, \boldsymbol{\upsilon}]$ need to include $\boldsymbol{\upsilon} = \{\boldsymbol{\zeta}, \mathbf{S}, \mathbf{S}_e\}$ because only the likelihood function $p(D|\boldsymbol{\alpha})$ has been derived in explicit analytical form.

The frequency bands for modal identification can be easily selected by the analyst based on a smoothed (averaged) version of the singular value spectrum computed from the time history data, e.g., see Figure 1, where there are $n_B = 3$ disjoint frequency bands. Within the r-th band, the FFT is modeled as

$$\hat{\mathcal{F}}_k = \mathcal{F}_k + \boldsymbol{\varepsilon}_k \tag{13}$$

where $\mathcal{F}_k$ is the theoretical modal response of the structure and $\boldsymbol{\varepsilon}_k$ is the prediction error (arising from, e.g., channel noise) in the frequency domain. The statistical properties of both $\mathcal{F}_k$ and $\boldsymbol{\varepsilon}_k$ depend on the modal parameters of the modes in the band.

At frequency f_k within the r-th selected band, the theoretical modal response is assumed to consist of the contributing modes in the band only, i.e.,

$$\mathcal{F}_k = \sum_{i=1}^{m_r} \boldsymbol{\Phi}_i^{(r)} \eta_{ik}^{(r)} \qquad \text{(within the } r\text{-th band)} \tag{14}$$

where the sum is over the modes in the r-th band whose number is m_r; $\boldsymbol{\Phi}_i^{(r)} \in R^n$ ($i = 1,...,m_r$) is the partial mode shape of the i-th mode in the r-th band; $\eta_{ik}^{(r)}$ is the FFT of the theoretical modal response of the i-th mode in the r-th band at frequency index k, whose time domain counterpart satisfies (4).

The prediction errors at different measured dofs are assumed to be independent and they have a constant PSD of $S_e^{(r)}$ in the r-th band. That is, they need not be 'white' over the whole sampling spectrum (from DC up to the Nyquist frequency), but only 'locally white' in the selected frequency bands. This is a robust assumption and is one advantage of operating in the frequency domain rather than the time domain.

Let $D^{(r)}$ denote the collection of the FFT data $\{\hat{\mathcal{F}}_k\}$ in the r-th frequency band. The set of modal parameters that completely characterizes the probability distribution of $D^{(r)}$ is

$$\boldsymbol{\alpha}^{(r)} = [\mathbf{f}^{(r)}, \boldsymbol{\Phi}^{(r)}, \boldsymbol{\zeta}^{(r)}, \mathbf{S}^{(r)}, S_e^{(r)}] \tag{15}$$

where

$$\mathbf{f}^{(r)} = [f_1^{(r)}, ..., f_{m_r}^{(r)}] \in R^{m_r} \tag{16}$$

$$\boldsymbol{\zeta}^{(r)} = [\zeta_1^{(r)}, ..., \zeta_{m_r}^{(r)}] \in R^{m_r} \tag{17}$$

denote respectively the set of natural frequencies and damping ratios for the modes in the band; $\mathbf{S}^{(r)} \in C^{m_r \times m_r}$ denotes the (Hermitian) PSD matrix of modal forces, assumed to be constant within the frequency band; $S_e^{(r)} \in R$ denotes the PSD of prediction error, assumed to be constant within the band; and

$$\boldsymbol{\Phi}^{(r)} = [\boldsymbol{\Phi}_1^{(r)}, ..., \boldsymbol{\Phi}_{m_r}^{(r)}] \in R^{n \times m_r} \tag{18}$$

denotes the partial mode shape matrix, assumed to be normalized with unit norm, i.e.,

$$\| \boldsymbol{\Phi}_i^{(r)} \|^2 = \boldsymbol{\Phi}_i^{(r)T} \boldsymbol{\Phi}_i^{(r)} = 1 \tag{19}$$

3.1 Likelihood function

The likelihood function for modal identification in Stage I corresponds to the PDF of the FFT in the selected frequency bands for a given $\boldsymbol{\alpha}$:

$$p(D \mid \boldsymbol{\alpha}) = P(D^{(1)}, ..., D^{(n_B)} \mid \boldsymbol{\alpha}) \tag{20}$$

It has been derived under asymptotic conditions for sufficiently high sampling rate and long data duration, which are often justified in applications [14][15][16]. Assuming stationary data, for a given $\boldsymbol{\alpha}$, the FFT data $\{D^{(r)} : r = 1, ..., n_B\}$ on different non-overlapping frequency bands are independent. This implies that

$$p(D \mid \boldsymbol{\alpha}) = \prod_{r=1}^{n_B} p(D^{(r)} \mid \boldsymbol{\alpha}) \tag{21}$$

Since the distribution of $D^{(r)}$ depends on $\boldsymbol{\alpha}^{(r)}$ only (see (14)),

$$p(D^{(r)} \mid \boldsymbol{\alpha}) = p(D^{(r)} \mid \boldsymbol{\alpha}^{(r)}) \tag{22}$$

and so

$$p(D \mid \boldsymbol{\alpha}) = \prod_{r=1}^{n_B} p(D^{(r)} \mid \boldsymbol{\alpha}^{(r)}) \tag{23}$$

The likelihood function $p(D^{(r)} \mid \boldsymbol{\alpha}^{(r)})$ corresponds to the one for a single frequency band:

$$p(D^{(r)} \mid \boldsymbol{\alpha}^{(r)}) \equiv p(\{\hat{\mathcal{F}}_k : k \in I_r\} \mid \mathbf{f}^{(r)}, \boldsymbol{\zeta}^{(r)}, \boldsymbol{\Phi}^{(r)}, \mathbf{S}^{(r)}, \mathbf{S}_e^{(r)}) \tag{24}$$

where I_r denotes the collection of the frequency indices in the r-th frequency band. It can be derived based on the following facts. It can be shown that the FFT $\hat{\mathcal{F}}_k$ at different frequencies are asymptotically independent. The real and imaginary part of $\hat{\mathcal{F}}_k$ follows a Gaussian distribution with zero mean and a covariance matrix that can be written in terms of $\boldsymbol{\alpha}^{(r)}$. The result is given by

$$p(D^{(r)} \mid \boldsymbol{\alpha}^{(r)}) \propto \exp[-L^{(r)}(\boldsymbol{\alpha}^{(r)})] \tag{25}$$

where

$$L^{(r)}(\boldsymbol{\alpha}^{(r)}) = \sum_{k \in I_r} \ln |\det \mathbf{E}_k^{(r)}| + \sum_{k \in I_r} \hat{\mathcal{F}}_k^* \mathbf{E}_k^{(r)-1} \hat{\mathcal{F}}_k \tag{26}$$

is the 'negative log-likelihood function' (NLLF); '*' denotes a complex conjugate transpose and 'det' denotes the determinant; and

$$\mathbf{E}_k^{(r)} = \boldsymbol{\Phi}^{(r)} \mathbf{H}_k^{(r)} \boldsymbol{\Phi}^{(r)T} + S_e^{(r)} \mathbf{I}_n \in C^{n \times n} \tag{27}$$

is a Hermitian matrix. In (27), $\mathbf{I}_n \in R^n$ denotes the identity matrix; $\mathbf{H}_k^{(r)} \in C^{m_r \times m_r}$ is the (Hermitian) transfer matrix of the modes in the r-th band and its (i, j)-entry is given by:

$$\mathbf{H}_k^{(r)}(i, j) = \mathbf{S}^{(r)}(i, j)[(\beta_{ik}^{(r)2} - 1) + \mathbf{i}(2\zeta_i^{(r)} \beta_{ik}^{(r)})]^{-1}[(\beta_{jk}^{(r)2} - 1) - \mathbf{i}(2\zeta_j^{(r)} \beta_{jk}^{(r)})]^{-1} \tag{28}$$

where

$$\beta_{ik}^{(r)} = \frac{f_i^{(r)}}{\mathrm{f}_k} \tag{29}$$

3.2 Hypothetical posterior distribution

Based on the standard form in (29) of the companion paper, the (hypothetical) posterior PDF $p_0(\boldsymbol{\alpha} \mid D)$ of the modal parameters in Stage I assuming a uniform prior distribution for ϖ is relevant in the two-stage identification process. Assuming a uniform prior distribution for $\boldsymbol{\upsilon}$ it is simply directly proportional to the likelihood function $p(D \mid \boldsymbol{\alpha})$. Using (23) and (25), it can be expressed as

$$p_0(\boldsymbol{\alpha} \mid D) \propto \prod_{r=1}^{n_B} p_0(\boldsymbol{\alpha}^{(r)} \mid D^{(r)}) \propto \exp[-\sum_{r=1}^{n_B} L^{(r)}(\boldsymbol{\alpha}^{(r)})] \tag{30}$$

where $L^{(r)}(\boldsymbol{\alpha}^{(r)})$ is given by (26).

Assuming each $\boldsymbol{\alpha}^{(r)}$ is globally identifiable (otherwise the modes will not be included for structural identification), the posterior PDF of each $\boldsymbol{\alpha}^{(r)}$ in (30) can be well-approximated by a Gaussian distribution centered at the most probable value (MPV) $\hat{\boldsymbol{\alpha}}^{(r)}$ and with a covariance matrix $\mathbf{C}^{(r)}$, i.e.,

$$p_0(\boldsymbol{\alpha}^{(r)} \mid D^{(r)}) = \phi(\boldsymbol{\alpha}^{(r)}; \hat{\boldsymbol{\alpha}}^{(r)}, \mathbf{C}^{(r)}) \tag{31}$$

Mathematically, the MPV $\hat{\boldsymbol{\alpha}}^{(r)}$ minimizes the NLLF in (26) subjected to norm constraints on the mode shapes in (19). The covariance matrix $\mathbf{C}^{(r)}$ is equal to the inverse of the Hessian of the NLLF evaluated at the MPV, ignoring the principle components along the most probable mode shape directions [17]. Efficient algorithms for computing the MPV and the covariance matrix has been developed [10][11][12][13].

Substituting (31) into (30) gives

$$p_0(\boldsymbol{\alpha} \mid D) \propto \prod_{r=1}^{n_B} \phi(\boldsymbol{\alpha}^{(r)}; \hat{\boldsymbol{\alpha}}^{(r)}, \mathbf{C}^{(r)}) \tag{32}$$

which is a joint Gaussian PDF for $\boldsymbol{\alpha} = [\boldsymbol{\alpha}^{(1)},...,\boldsymbol{\alpha}^{(n_B)}]$. Note that $\{\boldsymbol{\alpha}^{(r)} : r = 1,...,n_B\}$ for different bands are independent and within each band the mean and covariance matrix of $\boldsymbol{\alpha}^{(r)}$ are given by $\hat{\boldsymbol{\alpha}}^{(r)}$ and $\mathbf{C}^{(r)}$, respectively.

Due to the property of Gaussian distribution, the marginal posterior PDF of $\boldsymbol{\varpi} = \{\boldsymbol{\varpi}^{(r)}\}_{r=1}^{n_B}$ (a subset of the full set $\boldsymbol{\alpha} = [\boldsymbol{\varpi}, \boldsymbol{\upsilon}]$) is also Gaussian:

$$p_0(\boldsymbol{\varpi} \mid D) = \prod_{r=1}^{n_B} \phi(\boldsymbol{\varpi}^{(r)}; \hat{\boldsymbol{\varpi}}^{(r)}, \mathbf{C}_D^{(r)}) \tag{33}$$

where $\hat{\boldsymbol{\varpi}}^{(r)}$ and $\mathbf{C}_D^{(r)}$ denote the MPV and covariance matrix of $\boldsymbol{\varpi}$, respectively. They can be directly extracted from the corresponding partition of $\hat{\boldsymbol{\alpha}}^{(r)}$ and $\mathbf{C}^{(r)}$. Equation (33) can be written as

$$p_0(\boldsymbol{\varpi} \mid D) \propto \exp[-L_{\mathrm{I}}(\boldsymbol{\varpi})] \tag{34}$$

where

$$L_{\mathrm{I}}(\boldsymbol{\varpi}) = \frac{1}{2}\sum_{r=1}^{n_B} \ln \det \mathbf{C}_D^{(r)} + \frac{1}{2}\sum_{r=1}^{n_B} (\boldsymbol{\varpi}^{(r)} - \hat{\boldsymbol{\varpi}}^{(r)})^T \mathbf{C}_D^{-1} (\boldsymbol{\varpi}^{(r)} - \hat{\boldsymbol{\varpi}}^{(r)}) \tag{35}$$

Recall that $\hat{\boldsymbol{\varpi}}^{(r)}$ denotes the MPV of the natural frequencies and mode shapes in the r-th band; and $\mathbf{C}_D$ denotes the corresponding posterior covariance matrix. These are determined as part of the modal identification result in Stage I. The function $L_{\mathrm{I}}(\boldsymbol{\varpi})$ will be directly used for computation in Stage II later.

4 Structural model identification (Stage II)

In Stage II the structural modal parameters $\boldsymbol{\theta}$ are identified based on the structural prediction model in terms of $p(\boldsymbol{\varpi} \mid \boldsymbol{\theta})$ and the identification result in Stage I in terms of $p_0(\boldsymbol{\varpi} \mid D)$. In this work $\boldsymbol{\theta}$ is assumed to characterize $\boldsymbol{\varpi}$ through the stiffness matrix $\mathbf{K}$ and mass matrix $\mathbf{M}$ only. The dependence of the damping matrix $\mathbf{C}$ on $\boldsymbol{\theta}$ is not modeled. This is because in practice the interest is on the damping ratios $\boldsymbol{\zeta}$, which have already been identified in Stage I. Also, for full-scale structures the damping matrix is

much more difficult to model from mechanical principles than the stiffness matrix or mass matrix.

As mentioned in the introduction, the natural frequencies and mode shapes are assumed to be completely determined by the structural model parameters, in the sense that the conditional PDF $p(\varpi \mid \boldsymbol{\theta})$ is given by a Dirac-Delta function:

$$p(\varpi \mid \boldsymbol{\theta}) = \delta(\varpi - \tilde{\varpi}(\boldsymbol{\theta})) \tag{36}$$

where

$$\tilde{\varpi}(\boldsymbol{\theta}) = [\tilde{\mathbf{f}}(\boldsymbol{\theta}), \tilde{\boldsymbol{\Phi}}(\boldsymbol{\theta})] \tag{37}$$

comprises the theoretical natural frequencies $\tilde{\mathbf{f}}(\boldsymbol{\theta})$ and partial mode shapes $\tilde{\boldsymbol{\Phi}}(\boldsymbol{\theta})$ determined from the eigenvalue equation in (3) for given $\boldsymbol{\theta}$. In the current case, there is no parameters characterizing the uncertainty of the structural prediction error model and so in the context of Proposition 1 in the companion paper, $\boldsymbol{\theta}_S = \boldsymbol{\theta}$ and $\boldsymbol{\theta}_P$ is null. Substituting (34) and (36) into the standard form (12), the posterior distribution $p(\boldsymbol{\theta} \mid D)$ of the structural parameters is given by,

$$p(\boldsymbol{\theta} \mid D) \propto p(\boldsymbol{\theta}) \prod_{r=1}^{n_B} \phi(\tilde{\varpi}^{(r)}(\boldsymbol{\theta}); \hat{\varpi}^{(r)}, \mathbf{C}_D^{(r)}) \propto p(\boldsymbol{\theta}) \exp[-L_{\mathrm{II}}(\boldsymbol{\theta})] \tag{38}$$

where

$$L_{\mathrm{II}}(\boldsymbol{\theta}) = \frac{1}{2} \sum_{r=1}^{n_B} [\tilde{\varpi}^{(r)}(\boldsymbol{\theta}) - \hat{\varpi}^{(r)}]^T \mathbf{C}_D^{(r)^{-1}} [\tilde{\varpi}^{(r)}(\boldsymbol{\theta}) - \hat{\varpi}^{(r)}] \tag{39}$$

Note that the log-determinant term $\sum_{r=1}^{n_B} \ln \det \mathbf{C}_D^{(r)} / 2$ has been omitted in the above expression because it does not depend on $\boldsymbol{\theta}$. The form of $L_{\mathrm{II}}(\boldsymbol{\theta})$ resembles some measure-of-fit function between the MPV of the modal parameters $\hat{\varpi}$ and its model counterpart $\tilde{\varpi}(\boldsymbol{\theta})$. The quadratic nature of the discrepancy $[\tilde{\varpi}^{(r)}(\boldsymbol{\theta}) - \hat{\varpi}^{(r)}]$ stems from the Gaussian nature of the posterior distribution of modal parameters in Stage I.

In the general theory the conditional distribution $p(\varpi \mid \boldsymbol{\theta})$ can be a nontrivial probability distribution based on modeling by the analyst. The case considered here reflects that the

natural frequencies and mode shapes in Stage I are directly related to the structural model parameters without any structural modeling error. This is similar to what is considered in the existing literature. Nevertheless, the general theory provides a fundamental means for incorporating the structural modelling error through $p(\varpi \mid \boldsymbol{\theta})$. This modeling is related to the fidelity of the structural model under question and is left for future work.

4.1 Computational issue

Due to the norm constraint of the mode shapes, the covariance matrix $\mathbf{C}_D^{(r)}$ is singular with null vectors parallel to the most probable mode shapes [17]. For computational purpose it is necessary to bypass the numerical problems arising from evaluating the inverse $\mathbf{C}_D^{(r)^{-1}}$ in (39). This can be done by evaluating the inner product by summing contributions along the eigen basis of $\mathbf{C}_D^{(r)^{-1}}$. The details are explained as follows.

First note that the covariance matrix is equal to the inverse of the Hessian matrix of the NLLF in Stage I where the components along the most probable mode shape directions are omitted. If the r-th band contains m_r modes, $\mathbf{C}_D^{(r)}$ will have m_r zero eigenvalues with eigenvectors equal to the m_r most probable mode shapes obtained in Stage I. It can thus be expressed as

$$\mathbf{C}_D^{(r)} = \sum_{i=m_r+1}^{n_p^{(r)}} v_i^{(r)} \mathbf{b}_i^{(r)} \mathbf{b}_i^{(r)^T} \tag{40}$$

where $\{v_i^{(r)} : i = m_r + 1, ..., n_p^{(r)}\}$ are the non-zero eigenvalues of $\mathbf{C}_D^{(r)}$ with corresponding eigenvectors $\{\mathbf{b}_i^{(r)} \in R^{n_p^{(r)}} : i = m_r + 1, ..., n_p^{(r)}\}$; $n_p^{(r)} = m_r + m_r \times n$ is the number of modal parameters arising from the frequencies and mode shapes of the r-th selected band. Ignoring the components along the most probable mode shape directions, i.e., the m_r null vector directions, the inverse of $\mathbf{C}_D^{(r)}$ is given by

$$\mathbf{C}_D^{(r)^{-1}} = \sum_{i=m_r+1}^{n_p^{(r)}} v_i^{(r)^{-1}} \mathbf{b}_i^{(r)} \mathbf{b}_i^{(r)^T} \tag{41}$$

Substituting this into (39),

$$L_{\mathrm{II}}(\boldsymbol{\theta}) = \frac{1}{2} \sum_{r=1}^{n_B} \sum_{i=m_r+1}^{n_p^{(r)}} v_i^{(r)^{-1}} \{\mathbf{b}_i^{(r)^T} [\tilde{\varpi}^{(r)}(\boldsymbol{\theta}) - \hat{\varpi}^{(r)}]\}^2 \tag{42}$$

which no longer involves the inverse of the singular matrices $\{\mathbf{C}_D^{(r)} : r = 1,..., n_B\}$. As a remark, $\mathbf{C}_D^{(r)^{-1}}$ is just the partition of Hessian of the NLLF in Stage I corresponding to $\varpi^{(r)}$; $\{v_i^{(r)^{-1}}\}$ and $\{\mathbf{b}_i^{(r)}\}$ are the eigenvalues and eigenvectors of the Hessian.

4.2 Posterior statistics of structural model parameters

The posterior statistics of $\boldsymbol{\theta}$ can be determined from its posterior distribution in (38) where the NLLF is given by (42). In contrast to the modal identification problem in Stage I, the computational effort depends on whether the FFT data is sufficient for determining $\boldsymbol{\theta}$ or not. Specifically, if there exists a unique value of $\boldsymbol{\theta}$ that minimizes the NLLF, then the situation is 'globally identifiable' [18]. In this case, the MPV of $\boldsymbol{\theta}$ can be obtained by numerically minimizing the NLLF in (42) with respect to $\boldsymbol{\theta}$ using conventional optimization algorithms (e.g., simplex search). Under a second order Taylor approximation of the NLLF with respect to $\boldsymbol{\theta}$ about the MPV, the posterior covariance matrix of $\boldsymbol{\theta}$ can be determined as the inverse of Hessian of the NLLF at the MPV.

If the problem is not globally identifiable, the NLLF can either have multiple local (isolated) minima (i.e., locally identifiable) or even a manifold of stationary points (unidentifiable). Conventional optimization algorithms cannot be used for finding the critical points/regions that characterize the posterior distribution [19][20]. More advanced numerical tools such as Markov Chain Monte Carlo (MCMC) [21][22][23][24] may be pursued. Whenever feasible, it is better to avoid unidentifiable situations by choosing a simpler model, designing a better instrumentation layout, increasing the number of

measured dofs, etc. Despite the available advanced tools, studies on unidentifiable cases have so far been mostly of academic nature.

5 Comparison with conventional formulations

As mentioned in the introduction, Bayesian two-stage methods have been suggested previously. A common heuristic formulation (with variants) reflects in the likelihood function the discrepancy between the identified MPV and structural model prediction of the natural frequencies and partial mode shapes. The MPV of natural frequencies and mode shapes ($\hat{f}_i$ and $\hat{\boldsymbol{\Phi}}_i$) are assumed to be independent and related to their theoretical model counterparts ($\tilde{f}_i(\boldsymbol{\theta})$ and $\tilde{\boldsymbol{\Phi}}_i(\boldsymbol{\theta})$) by a prediction error, namely, for the i -th mode,

$$\begin{aligned} \hat{f}_i &= \tilde{f}_i(\boldsymbol{\theta}) + e_i \\ \hat{\boldsymbol{\Phi}}_i &= a_i(\boldsymbol{\theta})\tilde{\boldsymbol{\Phi}}_i(\boldsymbol{\theta}) + \mathbf{d}_i \end{aligned} \tag{43}$$

The term $e_i \in R$ is the prediction error for the natural frequency, assumed to be independent Gaussian among all modes, with zero mean and standard deviation σ_{fi}. The term $\mathbf{d}_i \in R^n$ is the prediction error for the mode shape, assumed to be independent Gaussian among all measured dofs and modes, with zero mean and standard deviation $\sigma_{\phi i}$. The factor a_i is chosen to scale the model mode shape for maximum likelihood (for given $\boldsymbol{\theta}$). The resulting posterior distribution is cast in the form $\exp[-J(\boldsymbol{\theta})]$ where

$$J(\boldsymbol{\theta}) = \frac{1}{2}\sum_i \sigma_{fi}^{-2}[\hat{f}_i - \tilde{f}_i(\boldsymbol{\theta})]^2 + \frac{1}{2}\sum_i \sigma_{\phi i}^{-2} \| \hat{\boldsymbol{\Phi}}_i - \hat{a}_i(\boldsymbol{\theta})\tilde{\boldsymbol{\Phi}}_i(\boldsymbol{\theta}) \|^2 \tag{44}$$

with the sums being over all identified modes; $\| \cdot \|$ denotes the Euclidean norm; $\| \hat{\boldsymbol{\Phi}}_i \| = 1$ and $\| \tilde{\boldsymbol{\Phi}}_i(\boldsymbol{\theta}) \| = 1$;

$$\hat{a}_i(\boldsymbol{\theta}) = \hat{\boldsymbol{\Phi}}_i^T \tilde{\boldsymbol{\Phi}}_i(\boldsymbol{\theta}) \tag{45}$$

is the optimized scaling constant that minimizes J for given $\boldsymbol{\theta}$. In [4][5] the first term was written as the squared difference of the squared natural frequencies but it is similar provided that the parameter σ_{fi} is assigned consistently. For implementation the values

of σ_{fi} and $\sigma_{\phi i}$ in (44) need to be set a priori, e.g., based on sample standard deviation of the corresponding MPV obtained from tests of similar configuration.

Expanding the norm in (44) and substituting (45), it can be readily shown that

$$J(\boldsymbol{\theta}) = \frac{1}{2}\sum_i \sigma_{fi}^{-2}[\hat{f}_i - \tilde{f}_i(\boldsymbol{\theta})]^2 + \frac{1}{2}\sum_i \sigma_{\phi i}^{-2}\{1-[\hat{\boldsymbol{\Phi}}_i^T \tilde{\boldsymbol{\Phi}}_i(\boldsymbol{\theta})]^2\} \quad (46)$$

Note that $\hat{\boldsymbol{\Phi}}_i^T \tilde{\boldsymbol{\Phi}}_i(\boldsymbol{\theta}) \in [-1,1]$ is the modal assurance criteria (MAC) between the model and most probable mode shape, assuming both have a unit norm.

In a more general setting, the measure of fit function $J(\boldsymbol{\theta})$ has been formulated as a weighted sum of normalized discrepancies in the frequencies and mode shapes among different modes [7][8]. It is found that the choice of the weights is closely related to the prediction error variance of the mode and they do have a significant effect on the MPVs. Even if the MPVs are insensitive to the weights, the same need not be true for the resulting posterior covariance matrix.

5.1 Underlying philosophy

The formulation proposed in this work and the conventional formulation adopt the same data prediction model in Stage I to relate the measured data (e.g., acceleration) to the theoretical dynamic response that depends on the modal parameters $\boldsymbol{\alpha}$. This allows the likelihood function $p(D|\boldsymbol{\alpha})$ to be explicitly derived, which yields the posterior distribution of $\boldsymbol{\alpha}$ in Stage I.

The major difference between the proposed and conventional formulation lies in the philosophy behind the structural prediction error that provides the link between Stage I and II. The conventional formulation adopts a structural prediction error model relating the posterior MPV of the modal parameters $\hat{\varpi}$ $(=[\hat{\mathbf{f}}, \hat{\boldsymbol{\Phi}}])$ to their theoretical model counterpart $\tilde{\varpi}(\boldsymbol{\theta})$ $(=[\tilde{\mathbf{f}}(\boldsymbol{\theta}), \tilde{\boldsymbol{\Phi}}(\boldsymbol{\theta})]$, see (43)). The rationale behind this is to treat the MPV of the modal parameter as a directly observed 'data' of the model counterpart. Modeling in this manner, the prediction error should generally account for both the uncertainty of

$\hat{\varpi}$ in Stage I and structural modeling error. The former is related to identification uncertainty in Stage I, though in a somewhat frequentist sense since it is associated with the descriptive statistic $\hat{\varpi}$ rather than directly with ϖ. The latter is related to fidelity of the finite element model. In this context, deriving from first principles the distribution of the structural prediction error and hence the distribution of $\hat{\varpi}$ for given $\boldsymbol{\theta}$ (required for Stage II) is highly non-trivial. Heuristics are therefore involved in assuming a reasonable distribution conducive for computations. As it turns out, the existing conventional formulations address mainly the identification uncertainty of in $\hat{\varpi}$ rather than the structural modeling uncertainty.

Casting a prediction error model on the descriptive statistics rather than on the parameter itself, as in the conventional formulations, distorts Bayesian probability logic. After all, the modal properties ϖ, i.e., the natural frequencies and mode shapes, are not directly 'observed'. The MPV $\hat{\varpi}$ is just a descriptive statistic convenient for characterizing the posterior distribution of ϖ in Stage I. It is ϖ that is identified, not $\hat{\varpi}$.

The proposed formulation adopts a more fundamental means of linking Stage I and II. It casts the structural prediction error model directly on the uncertain parameters ϖ and $\boldsymbol{\theta}$. Based on this, the conditional distribution $p(\varpi|\boldsymbol{\theta})$ can be rigorously derived, which is the fundamental mathematical object that describes structural modeling uncertainty. Methodologically, this conditional distribution does not depend on the identification uncertainty of ϖ in Stage I, making it easier to be formulated based on first principles. The application of the general theory to structural system identification based on ambient data in this paper specifically assumes no structural prediction error, which can be stated explicitly in the formulation of $p(\varpi|\boldsymbol{\theta})$ independent of the identification uncertainty of ϖ in Stage I implied by $p(\varpi|D)$. Finally, the information in $p(\varpi|\boldsymbol{\theta})$ is incorporated with the posterior distribution of ϖ in Stage I and other prior information to give the posterior distribution of $\boldsymbol{\theta}$, in strict accordance with probability logic. No frequentist concepts are involved.

5.2 Similar quantitative results under specific conditions

Despite the criticisms in the last section, we provide an argument here that shows the conventional formulation yields identification results that are quantitatively similar to the proposed formulation when

1) there is no structural prediction error, i.e., $p(\varpi \mid \boldsymbol{\theta}) = \delta(\varpi - \tilde{\varpi}(\boldsymbol{\theta}))$;
2) the modes are well-separated;
3) the ambient data has high modal signal-to-noise ratios;
4) the parameters $\{\sigma_{fi}\}$ and $\{\sigma_{\phi i}\}$ are assigned based on the posterior uncertainty of the natural frequencies and mode shapes in Stage I, specifically, according to (52).

That is, although the existing formulations are heuristic, they are well-thought. The intention here is to provide a meeting point for the proposed and conventional formulation so that future developments and results of the former can be explored leveraging on the past experience accumulated with the latter.

Specifically, we show that under the above conditions the NLLF $L_{\mathrm{II}}(\boldsymbol{\theta})$ in (39) reduces to $J(\boldsymbol{\theta})$ in (46). The first condition has been assumed throughout this paper. Under the second and third condition, the posterior uncertainty of the modal parameters obey the uncertainty laws of ambient modal identification [25][26], in which case $L_{\mathrm{II}}(\boldsymbol{\theta})$ reduces to the same form as $J(\boldsymbol{\theta})$. The last condition matches their coefficients.

For well-separated modes each band contains only one mode. When the modal s/n ratio is high, the posterior covariance matrix of the modal parameters is given by their uncertainty laws. In this case, the natural frequencies and modes shapes are independent. The posterior covariance matrix $\mathbf{C}_D$ in (39) reduces to a block-diagonal matrix. For the i-th mode it is asymptotically given by

$$\mathbf{C}_D^{(i)} = \begin{bmatrix} \hat{\sigma}_{fi}^2 & \\ & \hat{\mathbf{C}}_{\boldsymbol{\Phi}_i} \end{bmatrix} \tag{47}$$

where $\hat{\sigma}_{fi}^2$ is the posterior variance of the natural frequency f_i; and $\hat{\mathbf{C}}_{\mathbf{\Phi}_i}$ is the posterior covariance matrix of $\mathbf{\Phi}_i$ given by

$$\hat{\mathbf{C}}_{\mathbf{\Phi}_i} = \frac{\delta_{\Phi i}^2}{(n-1)}[\mathbf{I}_n - \hat{\mathbf{\Phi}}\hat{\mathbf{\Phi}}^T] \tag{48}$$

and $\delta_{\Phi_i}^2$ is the sum of eigenvalues of $\hat{\mathbf{C}}_{\mathbf{\Phi}_i}$. Substituting (47) into (39) gives

$$L_{\mathrm{II}}(\boldsymbol{\theta}) = \frac{1}{2}\sum_i \hat{\sigma}_{fi}^{-2}[\hat{f}_i - \tilde{f}_i(\boldsymbol{\theta})]^2 + \frac{1}{2}\sum_i \mathbf{\Phi}_i^T \hat{\mathbf{C}}_{\mathbf{\Phi}_i}^{-1} \mathbf{\Phi}_i^T \tag{49}$$

Due to the norm constraint $\| \mathbf{\Phi}_i \| = 1$, $\hat{\mathbf{C}}_{\mathbf{\Phi}_i}$ is singular along the direction $\hat{\mathbf{\Phi}}_i$ and its inverse should be evaluated ignoring this direction. This gives

$$\hat{\mathbf{C}}_{\mathbf{\Phi}_i}^{-1} = \frac{n-1}{\delta_{\Phi i}^2}[\mathbf{I}_n - \hat{\mathbf{\Phi}}\hat{\mathbf{\Phi}}^T] \tag{50}$$

Substituting into (49) gives

$$L_{\mathrm{II}}(\boldsymbol{\theta}) = \frac{1}{2}\sum_i \hat{\sigma}_{fi}^{-2}[\hat{f}_i - \tilde{f}_i(\boldsymbol{\theta})]^2 + \frac{1}{2}\sum_i \frac{n-1}{\delta_{\Phi i}^2}\{1 - [\hat{\mathbf{\Phi}}_i^T \tilde{\mathbf{\Phi}}_i(\boldsymbol{\theta})]^2\} \tag{51}$$

Comparing (51) and (46), we see that $J(\boldsymbol{\theta}) \equiv L_{\mathrm{II}}(\boldsymbol{\theta})$ when the prediction error variances in the conventional formulation are assigned as, for all the identified modes,

$$\begin{aligned} \sigma_{fi}^2 &= \hat{\sigma}_{fi}^2 \\ \sigma_{\phi i}^2 &= \frac{\delta_{\Phi i}^2}{n-1} \end{aligned} \tag{52}$$

Again, the above only provides an argument to suggest that the conventional formulation can give reasonable identification results under the specific conditions mentioned in the beginning of this section. Because of their heuristic nature, however, they are not recommended.

6 Summary of procedure

The proposed two-stage Bayesian structural system identification procedure, assuming no structural prediction error and based on ambient vibration data, is presented as follows. The overall objective is to obtain the posterior statistics of the set of structural model parameters $\boldsymbol{\theta}$ given the FFT data on selected frequency band(s) of the ambient acceleration data $\{\hat{\mathbf{y}}_j\}$ at the measured dofs.

Stage I

For each frequency band, $r = 1,...,n_B$, perform Bayesian modal identification to determine the MPV $\varpi^{(r)} = [\hat{\mathbf{f}}^{(r)}, \hat{\boldsymbol{\Phi}}^{(r)}]$ and the posterior covariance matrix $\hat{\mathbf{C}}_D^{(r)} \in R^{m_r(n+1)\times m_r(n+1)}$ of the natural frequencies and mode shapes. Details are referred to [10][11] for well-separated modes and [12][13] for general multiple (possibly close) modes.

Stage II

Determine the posterior statistics of the set of structural model parameters $\boldsymbol{\theta}$ based on the NLLF in (42). For globally identifiable cases, the posterior statistics may be obtained in terms of the MPV and the posterior covariance matrix of $\boldsymbol{\theta}$. The MPV can be found by numerically minimizing the NLLF. The posterior covariance matrix is equal to the inverse of the Hessian of the NLLF with respect to $\boldsymbol{\theta}$ and evaluated at the MPV. Finite difference method may be used if analytical expressions are not available. For globally unidentifiable cases, more advanced numerical tools such as MCMC [23] may be used. Practically it is better to avoid unidentifiable situations by choosing a simpler model or improving the test configuration, e.g., better sensor locations, more sensors, etc.

7 Illustrative applications

Two examples are presented to illustrate the proposed method and its applications. The first example is based on synthetic data and serves to verify the proposed method. The second example is based on experimental data and illustrates application in the real setting. The examples are all globally identifiable and so the posterior distribution of the

parameters can be characterized through their posterior MPV and covariance matrix. Unidentifiable cases require special attention and are out of the scope of this section. Unless otherwise stated, a uniform prior distribution is assumed for the modal parameters (Stage I) and structural model parameters (Stage II).

7.1 One-storied shear building (synthetic data)

Consider a one-storied shear building in Figure 2 supported on four columns, C1 to C4. The roof has a mass of 500 tons. Its mass moment of inertia about the center of mass is calculated to be $33333\,ton \cdot m^2$. The mass of the columns are assumed to be negligible. The lateral stiffness of the columns are shown in Table 1. Assuming rigid floor, the structure has three dofs, i.e., translations along the x and y direction and a rotation. The natural frequencies are calculated to be 8.016Hz (x-translation), 11.027Hz (y-translation) and 16.816Hz (rotation). Classical damping is assumed with a damping ratio of 1% in all modes. The building is subjected to ambient excitation at the roof modeled by independent and identically distributed (i.i.d.) Gaussian white noise in the x, y and rotational direction, with a one-sided root PSD of $1\,N/\sqrt{Hz}$, $0.9\,N/\sqrt{Hz}$ and 6 $Nm/\sqrt{Hz}$, respectively. Calculated using a sampling rate of 200Hz, the resulting acceleration response is in the order of a few tens of $\mu g/\sqrt{Hz}$ at resonance. The acceleration data is contaminated by measurement noise modeled by Gaussian white noise with a root PSD of $2\,\mu g/\sqrt{Hz}$.

7.1.1 Nominal case

We first consider a nominal scenario, based on which further discussions are expanded later. In this case, horizontal bi-axial acceleration measurement for 180 seconds is assumed to be available at the four columns on the roof as shown in Figure 2, giving a total of 8 measured dofs. Figure 1 shows the root PSD and root singular value (SV) spectra calculated using the ambient data. These smoothed (averaged) spectra are used for visualization only. They are not involved in the Bayesian modal identification process as the raw FFTs are used. In Figure 1, there are clear spectral peaks indicating structural modes near 8Hz, 11Hz and 17Hz. It is apparent that the noise floor in the PSD is about 2 $\mu g/\sqrt{Hz}$, which checks with the value assumed. In the SV spectrum the number next to

each peak shows the mode number. The horizontal bar shows the frequency band whose FFTs is used for identifying the mode within the band. The circle indicates the initial guess of natural frequency used for numerical optimization in the search of the MPV. Modal identification is performed for each band separately.

Table 2 shows the identification result for the modal parameters (Stage I) in terms of their posterior most probable values (MPV) and coefficient of variation (c.o.v.=standard deviation/MPV). Their 'exact' values used for generating the data are also shown. The MPVs are close to their exact values in a manner consistent with their posterior c.o.v.s. The Modal Assurance Criteria (MAC) between the identified and exact mode shapes are also shown in the table under the column 'MAC'. They are all very close to 1, suggesting a close agreement. The last column in the table quantifies the mode shape uncertainty in terms of the complement of the Expected MAC (EMAC) value (the lower the better) [17]. The EMAC is computed based on a single set of data only and it does not require information of the 'exact' mode shape. Generally, the posterior uncertainty of the natural frequencies and mode shapes are much smaller than those of the damping ratios.

The modal identification results are next used for identifying the interstory stiffness. The mass properties are assumed to be known and equal to the values that generated the data. The structural model used for identification is a simplified version of the original structure through the following parameterization based on the nominal values in Table 1 (all in kN/mm):

$$\begin{aligned} k_{x1} &= k_{x4} = 400\theta_{x1} \\ k_{x2} &= k_{x3} = 250\theta_{x2} \\ k_{y1} &= k_{y4} = 600\theta_{y1} \\ k_{y2} &= k_{y3} = 600\theta_{y2} \end{aligned} \tag{53}$$

Here,

$$\boldsymbol{\theta} = [\theta_{x1}, \theta_{x2}, \theta_{y1}, \theta_{y2}] \tag{54}$$

is the set of (dimensionless) structural model parameters to be identified in Stage II. All the three modes identified in Stage I are used for identifying $\boldsymbol{\theta}$ in Stage II.

Figure 3 summarizes the identification results in Stage II. Each parameter is shown with a dot at the MPV and an error bar covering +/- 2 posterior standard deviations. The dashed line shows the exact value. The error bars cover the exact value in all cases, suggesting that there is no bias in the identification. To examine whether the most probable structural model in Stage II results in modal properties consistent with the identification results in Stage I, Figure 4 shows the natural frequencies of the most probable structural model ('O'), the identification result in Stage I (dot and +/- 2 standard deviation error bar) and the exact value that generated the data (dashed line). The crosses are within the error bars and almost coincide with the dots, reflecting a good agreement in the modal properties between Stage I and Stage II. This is further confirmed by Figure 5 that compares the most probable mode shapes in Stage I and the mode shapes resulting from the most probable structural model in Stage II. Their MAC is very close to 1, typically in excess of 99%.

7.1.2 Effect of alignment error

We next investigate the effect of sensor alignment error on the identification of the stiffness parameters. This is motivated by the problems encountered in real situations where alignment error is inevitable. Let $\ddot{u}$ and $\ddot{v}$ denote the acceleration at a given point along the x and y direction, respectively. When subjected to an alignment error of Δ (clock-wise positive, in radian), the measured acceleration data $\hat{\ddot{u}}$ and $\hat{\ddot{v}}$ along the x and y direction are respectively given by

$$\begin{aligned} \hat{\ddot{u}} &= \ddot{u}\cos\Delta - \ddot{v}\sin\Delta \\ \hat{\ddot{v}} &= \ddot{u}\sin\Delta + \ddot{v}\cos\Delta \end{aligned} \tag{55}$$

A random alignment error Δ uniformly distributed between +/- 10 degree is introduced to the synthetic data (independent for different bi-axial sensors), in addition to the sensor noise considered in the nominal case. This introduces error in the mode shapes but not the natural frequencies.

Figure 6 shows the identified stiffness in Stage II, in a manner analogous to Figure 3. Different from Figure 3, the error bars do not cover the dashed lines, reflecting a potential

bias. This is thought to be due to the alignment error. Figure 7 compares the most probable mode shapes in Stage I and the theoretical mode shapes resulting from the most probable structural model in Stage II. The mode shapes on the right column satisfy rigid floor assumption, as they are calculated from the most probable structural model. The same is not true for the most probable mode shapes on the left column, as the data they are identified from are contaminated by alignment error. Note that the identified mode shapes have similar posterior uncertainty (not presented here) as their counterparts in Figure 5 because the alignment error does not change the spectral characteristics of the data used for modal identification in Stage I. There is no structural model within the model class considered in Stage II that will have mode shapes fitting reasonably well the identified mode shapes in Stage I, however. The most probable structural model in Stage II tries to accomplish this within the model class and this leads to bias.

7.2 Laboratory shear frame (real experimental data)

The proposed method is next investigated with real experimental data from a laboratory shear frame model as shown in Figure 8(a). The story heights are (from bottom to top) 858mm, 571mm and 555mm. All column sections measure 5mm by 25mm. The picture shows the weak (x) direction of the frame. Each floor measures 450mm×280mm×25mm and weighs 25.2 kg. The mass moment of inertia is calculated to be $0.59\,kg\cdot m^2$.

Assuming an elastic modulus of $1.55\times10^{11}N/m^2$, the interstory stiffness along the weak and strong directions are calculated and shown in Table 3.

7.2.1 Modal identification (Stage I)

The acceleration at the four corners of each floor were measured bi-axially along the horizontal direction, resulting in 24 measured dofs. Digital acceleration time history data of 600 seconds duration were originally acquired at 2048Hz and later decimated by 8 to 256Hz for modal identification. Figure 9 shows the root PSD and root SV spectra of the measured data. The nature of the mode associated with each spectral peak is indicated, e.g., 'TX2' for the second translational mode along the x direction and 'R3' for the third rotational mode. The modal identification results are shown in Table 4. The most probable mode shapes are shown in Figure 10. Generally the modes are well-identified and their identification uncertainty is small. As a remark, the mode at about 35Hz in

Figure 9 is excluded from analysis because it is found not to be associated with shear building dynamics considered within the structural model class in Stage II.

7.2.2 Structural model identification (Stage II)

In Stage II, the stiffness of the columns are identified. The mass properties are assumed to be equal to the nominal properties of the floors, ignoring the mass of the columns. The lateral stiffness of the four columns in each story are assumed to be identical and equal to a quarter of the total interstory stiffness. For the i-th story ($i=1,2,3$), the interstory stiffness along the x direction, k_{xi}, and y direction, k_{yi}, are parameterized by

$$\begin{aligned} k_{xi} &= \theta_{xi}\bar{k}_{xi} \\ k_{yi} &= \theta_{yi}\bar{k}_{yi} \end{aligned} \tag{56}$$

where $\bar{k}_{xi}$ and $\bar{k}_{yi}$ denote respectively the nominal value of interstory stiffness along the x and y direction as given in Table 3. Here,

$$\boldsymbol{\theta} = [\theta_{x1}, \theta_{x2}, \theta_{x3}, \theta_{y1}, \theta_{y2}, \theta_{y3}] \tag{57}$$

is the set of (dimensionless) structural model parameters to be identified in Stage II.

7.2.3 Nominal case

In the nominal case, the data at all the 24 measured dofs are used for modal identification in Stage I and model identification in Stage II. Table 5 shows the identification results in Stage II. Except for θ_{x1}, the stiffness parameters generally have a MPV close to 1 with a small c.o.v., reflecting that the actual stiffness properties are similar to what were predicted based on the available nominal information. The abnormally low value of θ_{x1} may be attributed to the reduction in stiffness due to the hole in the column (Figure 8(b)), which has been ignored in the calculation of the nominal stiffness. The posterior c.o.v. of the stiffness parameters are all very small. This is attributed to the small posterior c.o.v. of the modal parameters in Stage I.

7.2.4 Effect of the number of identified modes

We next investigate the effect of the number of modes used for structural model identification in Stage II. For this purpose, the number of modes included in the NLLF (39) in Stage II is incrementally increased, starting from the lower modes. Figure 11 shows the identification results in terms of the most probable values (dots) and error bars

covering +/- 2 standard deviations. For the stiffness in the x (weak) direction, e.g., θ_{x1}, the posterior uncertainty is significantly reduced as the number of modes is increased from one to two. Starting from four modes there is little change in the identification results. This may be attributed to the fact that the three modes along the x-direction correspond to modes 1, 2 and 4, and so the effect of the additional information after four modes is marginal. The effect of adding modes on the identification result of the stiffness along the y-direction is more significant, recognizing that the three modes (TY1, TY2, TY3) correspond to modes 3, 6 and 8. The stiffness along the y-direction is not identified when only up to the first two modes (TX1, TX2) are used because in that case they cannot be identified.

7.2.5 Effect of the number of measured dofs

We next investigate the effect of the number of measured dofs. For this purpose, we perform Stage I and Stage II for data with different measured dofs. In all cases the first six modes are included for identification. The identification results of the stiffness parameters are shown in Figure 12. Case 1 corresponds to the nominal case in Section 7.2.3 where the data at all the four columns and all floors are used, i.e., a total of 24 measured dofs. Case 2 reduces the number of measured dofs by half by using only the data on the two columns on the left of Figure 8(a). From Figure 12, this leads to a slight increase in the posterior uncertainty in the stiffness parameters but no significant change in their MPVs. Case 3 to Case 5 further reduce the number of dofs by using the data on only two floors. In all these cases it is found that the identification results can differ significantly depending on the information used. The error bars in different cases do not necessarily overlap each other.

8 Conclusions

A fundamental two-stage formulation for structural system identification has been presented in this work where the modal properties are identified using Fast Bayesian FFT method with ambient data. The structural prediction error is fundamentally quantified in terms of the conditional distribution of the modal parameters for given structural model parameters, which can be formulated independent of the identification uncertainty of the

modal parameters. In contrast with the conventional formulation, the resulting posterior distribution of the structural parameters is in strict accordance with Bayesian probability logic without heuristics or frequentist concepts. Although the method in this paper focuses on the case of ambient data, it can be readily adapted to the case of identification with known input excitation within the general framework developed in the companion paper.

The proposed method has been investigated using synthetic and laboratory data. Studies have been carried out to illustrate the effect of available information in terms of the number of measured dofs and the number of modes. The results reveal that the structural model identification results in Stage I can different significantly depending on the information (e.g., modes, measured dofs) used for identification. Bearing in mind that the posterior distribution of the model parameters are always conditional on the model used, this can be a reflection of structural modeling error, which has been assumed to be zero in the study. One natural future direction would be to incorporate structural modeling error through the conditional distribution $p(\varpi \mid \boldsymbol{\theta})$ in the general framework.

9 Acknowledgements

The work in this paper is partially supported by Grant EGG10034 from the University of Liverpool, the National Basic Research Program of China (973 Program) (Project No. 2014CB049100) and Fundamental Research Funds for the Central Universities, China (Grant No. 2014KJ040).

References

[1] S.K. Au, F.L. Zhang, A Fundamental Two-Stage Formulation for Bayesian System Identification, Part I: General Theory, Mechanical Systems and Signal Processing (2014).
[2] H. Wenzel, D. Pichler, Ambient vibration monitoring, John Wiley & Sons, UK, 2005.
[3] J.M.W. Brownjohn, A. De Stefano, Y.L. Xu, H. Wenzel, A.E. Aktan, Vibration-based monitoring of civil infrastructure: challenges and successes, Journal of Civil Structural Health Monitoring, 1(3-4)(2011) 79-95.
[4] M.W. Vanik, J.L. Beck, S.K. Au. Bayesian Probabilistic Approach to Structural Health Monitoring, Journal of Engineering Mechanics, ASCE 126(7)(2000) 738-745.

[5] J.L. Beck, S.K. Au, M.W. Vanik, Monitoring Structural Health Using a Probabilistic Measure, Computer-Aided Civil and Infrastructure Engineering, 16(1) (2001) 1-11.
[6] K.V. Yuen, J.L. Beck, L.S. Katafygiotis, Efficient Model Updating and Health Monitoring Methodology Using Incomplete Modal Data without Mode Matching, Structural Control and Health Monitoring 13(2006) 91-107.
[7] K. Christodoulou, C. Papadimitriou, Structural Identification Based on Optimally Weighted Modal Residuals, Mechanical Systems and Signal Processing, 21(2007) 4-23.
[8] K. Christodoulou, E. Ntotsios, C. Papadimitriou, C. Panetsos, Structural Model Updating and Prediction Variability Using Pareto Optimal Models, Computational Methods and Applications in Mechanical Engineering, 198(2008) 138-149.
[9] H.F. Lam, H.Y. Peng and S.K. Au (2014), Development of a practical algorithm for Bayesian model updating of a coupled slab system utilizing field test data, Engineering Structures, 79(2014): 182-194.
[10] S.K. Au, Fast Bayesian FFT Method for Ambient Modal Identification with Separated Modes, Journal of Engineering Mechanics, ASCE 137(3)(2011) 214-226.
[11] F.L. Zhang, S.K. Au, Erratum for "Fast Bayesian FFT Method for Ambient Modal Identification with Separated Modes" by S. K. Au, Journal of Engineering Mechanics, ASCE 139(4)(2013) 545-545.
[12] S.K. Au, Fast Bayesian Ambient Modal Identification in the Frequency Domain, Part I: Posterior Most Probable Value, Mechanical Systems and Signal Processing 26(2012) 60-75.
[13] S.K. Au, Fast Bayesian Ambient Modal Identification in the Frequency Domain, Part II: Posterior Uncertainty, Mechanical Systems and Signal Processing, 26(2012) 76-90.
[14] S.K. Au, F.L. Zhang, Y.C. Ni, Bayesian Operational Modal Analysis: Theory, Computation, Practice, Computers and Structures, 126(2013) 3-14.
[15] K.V. Yuen, L.S. Katafygiotis, Bayesian Fast Fourier Transform Approach for Modal Updating Using Ambient Data, Advances in Structural Engineering, 6(2)(2003) 81-95.
[16] J. Schoukens, R. Pintelon, Identification of Linear Systems: A Practical Guideline for Accurate Modeling, Pergamon Press, London, 1991.
[17] S.K. Au, F.L. Zhang, On Assessing Posterior Mode Shape Uncertainty in Ambient Modal Identification, Probabilistic Engineering Mechanics 26(3)(2011) 427-434.
[18] J.L. Beck, L.S. Katafygiotis, Updating Models and Their Uncertainties. I: Bayesian Statistical Framework, Journal of Engineering Mechanics, ASCE 124(4)(1998) 455-461.
[19] L.S. Katafygiotis, C. Papadimitriou, H.F. Lam, A Probabilistic Approach to Structural Model Updating, Soil Dynamics & Earthquake Engineering 17(7-8)(1998) 495-507.

[20] L.S. Katafygiotis and H.F. Lam, Tangential-Projection Algorithm for Manifold Representation in Unidentifiable Model Updating Problems, Earthquake Engineering & Structural Dynamics 31(4)(2002) 791-812.

[21] J.L. Beck, S.K. Au, Bayesian Updating of Structural Models and Reliability Using Markov Chain Monte Carlo Simulation, Journal of Engineering Mechanics, ASCE 128(4)(2002) 380-391.

[22] J. Ching, Y.C. Chen, Transitional Markov Chain Monte Carlo Method for Bayesian Updating, Model Class Selection, and Model Averaging, Journal of Engineering Mechanics, ASCE 133(2007) 816-832.

[23] C. Robert, G. Casella, Monte Carlo Statistical Methods. New York: Springer, 1999.

[24] D. Straub and I. Papaioannou, Bayesian Updating with Structural Reliability Methods, Journal of Engineering Mechanics (2014). Accepted for publication.

[25] S.K. Au, Uncertainty Law in Ambient Modal Identification. Part I: Theory, Mechanical Systems and Signal Processing 48(1-2) (2014)15-33.

[26] S.K. Au, Uncertainty Law in Ambient Modal Identification. Part II: Implication and Field Verification, Mechanical Systems and Signal Processing 48(1-2) (2014) 34-48.

List of tables

Table 1 Lateral stiffness of columns, one-storied building
Table 2 Identified modal parameters (Stage I), one-storied building, nominal case
Table 3 Nominal value of interstory stiffness, laboratory frame
Table 4 Identified modal parameters (Stage I), laboratory frame
Table 5 Identified stiffness parameters (Stage II), laboratory frame, nominal case

List of figures

Figure 1 Root PSD and root SV spectra, one-storied building
Figure 2 Plan view of one-storied building
Figure 3 Identified stiffness parameters (Stage II), one-storied building, nominal case
Figure 4 Comparison of natural frequencies. Identification results (Stage I, dot and +/-2 standard deviation error bar), most probable structural model (Stage II, 'O'), and exact value (dash line)
Figure 5 Comparison of mode shapes, one-storied building, nominal case. Left – MPV identified in Stage I; Right – resulting from the most probable structural model in Stage II
Figure 6 Identified stiffness parameters in Stage II, one-storied building, with alignment error
Figure 7 Comparison of mode shapes, one-storied building with alignment error. Left – MPV identified in Stage I; Right – resulting from the most probable structural model in Stage II
Figure 8 Laboratory model. (a) Overview; (b) Hole in the front left column on the first floor.
Figure 9 Root PSD and root SV spectra, laboratory frame
Figure 10 Most probable mode shapes, laboratory frame
Figure 11 Identified stiffness parameters (MPV and +/- 2 standard deviations) based on different number of modes
Figure 12 Identified stiffness parameters (MPV and +/- 2 standard deviations) based on different measured dofs, including the first six modes. Case 1: four columns, 1-3/F; Case 2: two columns on the left, 1-3/F; Case 3: two columns on the left, 1/F & 2/F; Case 4: two columns on the left, 1/F & 3/F; Case 5: two columns on the left, 2/F & 3/F.

Table 1 Lateral stiffness of columns, one-storied building

Column	Direction x (kN/mm)	Direction y (kN/mm)
1	400	600
2	250	600
3	250	600
4	400	600

Table 2 Identified modal parameters (Stage I), one-storied building, nominal case

Mode	Natural frequency (Hz)			Damping ratio (%)			Mode shape	
	Exact	Identified		Exact	Identified			1-EMAC
		MPV	c.o.v. (%)		MPV	c.o.v. (%)	MAC	($\times 10^{-3}$)
1	8.016	8.017	0.12	1.00	0.90	13.83	0.9998	0.360
2	11.027	11.036	0.11	1.00	1.03	11.44	0.9997	0.348
3	16.816	16.813	0.09	1.00	1.11	8.50	0.9999	0.112

Table 3 Nominal value of interstory stiffness, laboratory frame

Story	Direction x (N/mm)	Direction y (N/mm)
1	3.07	76.69
2	10.41	260.18
3	11.33	283.34

Table 4 Identified modal parameters (Stage I), laboratory frame

Mode	Nature	Natural frequency		Damping ratio		Mode shape 1-EMAC ($\times 10^{-6}$)
		MPV (Hz)	c.o.v. (%)	MPV (%)	c.o.v. (%)	
1	TX1	0.808	0.09	0.25	39.3	945.9
2	TX2	3.523	0.03	0.12	26.0	12.5
3	TY1	4.822	0.02	0.06	29.6	6.8
4	TX3	5.902	0.02	0.11	20.9	5.9
5	R1	7.105	0.02	0.15	16.0	2.0
6	TY2	17.659	0.01	0.13	11.2	17.0
7	R2	26.373	0.02	0.25	6.6	3.5
8	TY3	31.489	0.01	0.07	11.0	6.7
9	R3	45.861	0.01	0.12	7.1	1.1

Table 5 Identified stiffness parameters (Stage II), laboratory frame, nominal case

Story i	θ_{xi}	θ_{yi}
	MPV (c.o.v.)	MPV (c.o.v.)
1	0.7001 (0.21%)	1.0152 (0.03%)
2	1.0107 (0.08%)	1.1829 (0.06%)
3	1.0776 (0.07%)	1.1180 (0.06%)

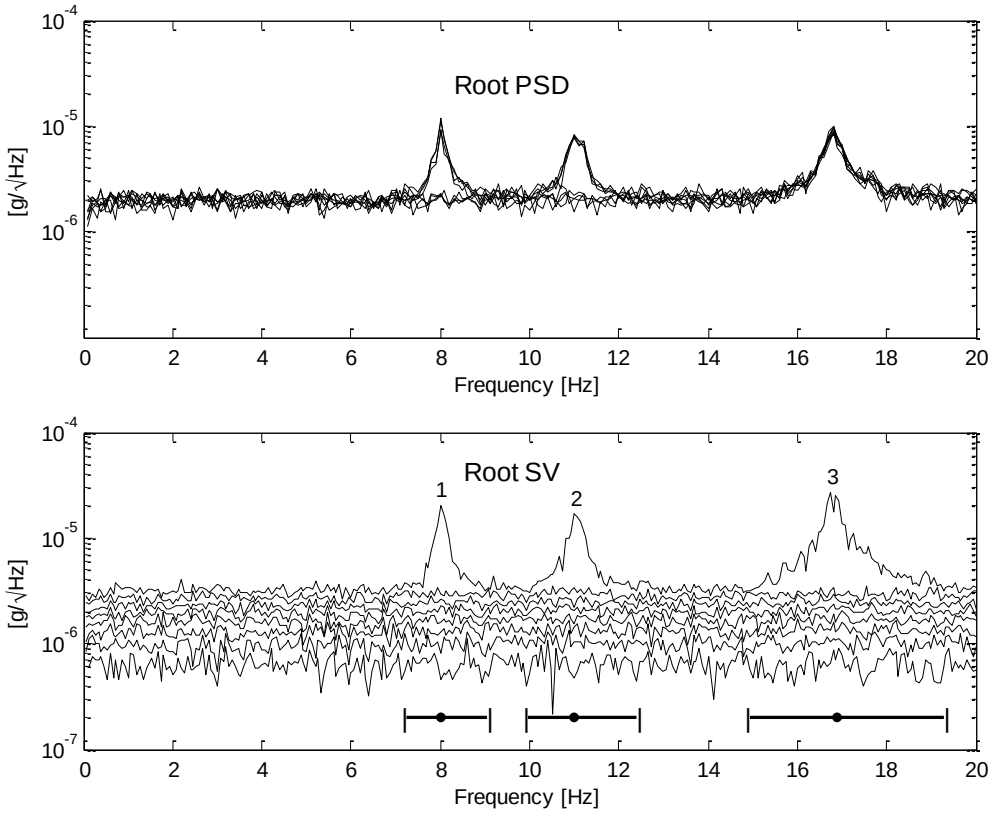

Figure 1 Root PSD and root SV spectra, one-storied building

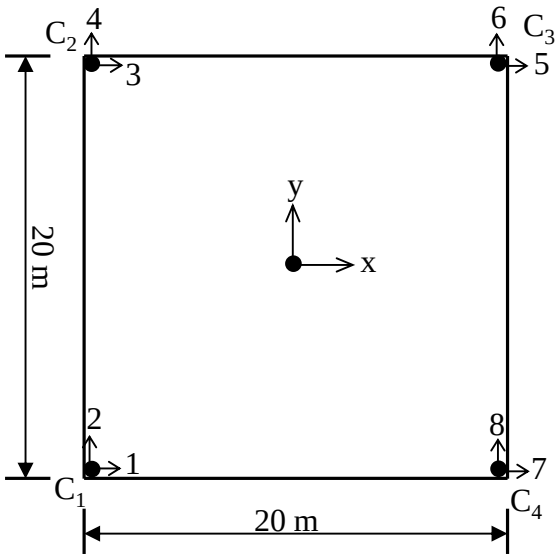

Figure 2 Plan view of one-storied building

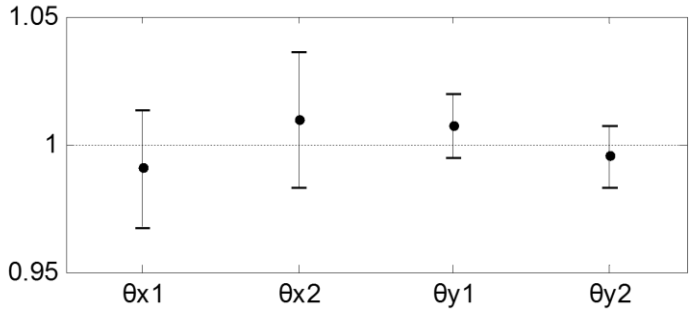

Figure 3 Identified stiffness parameters (Stage II), one-storied building, nominal case

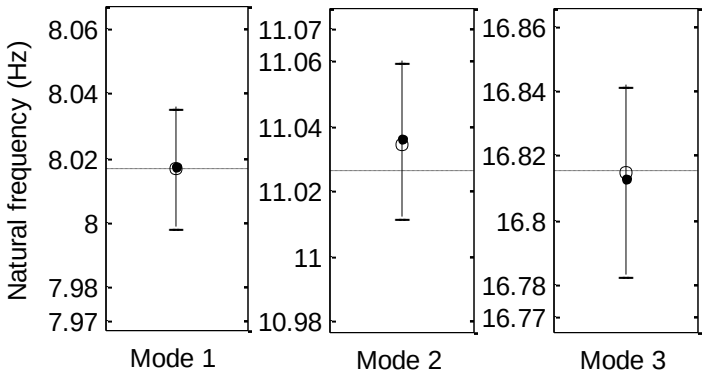

Figure 4 Comparison of natural frequencies. Identification results (Stage I, dot and +/-2 standard deviation error bar), most probable structural model (Stage II, 'O'), and exact value (dash line)

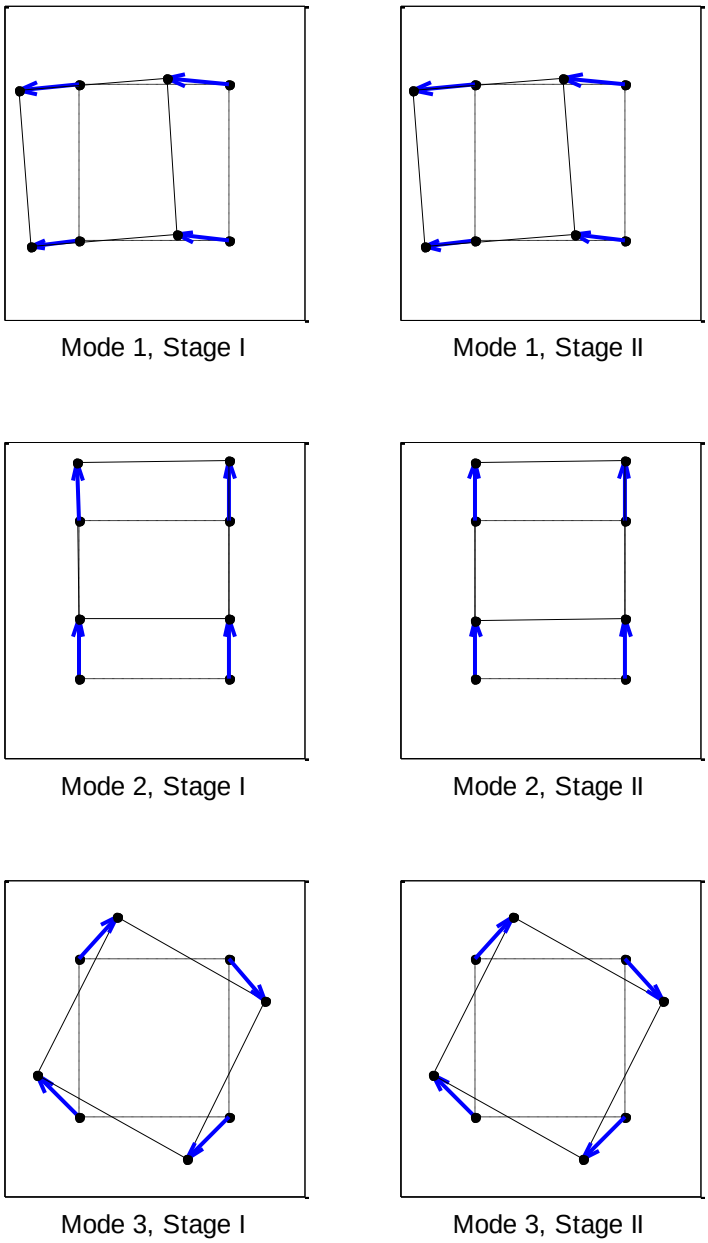

Figure 5 Comparison of mode shapes, one-storied building, nominal case. Left – MPV identified in Stage I; Right – resulting from the most probable structural model in Stage II

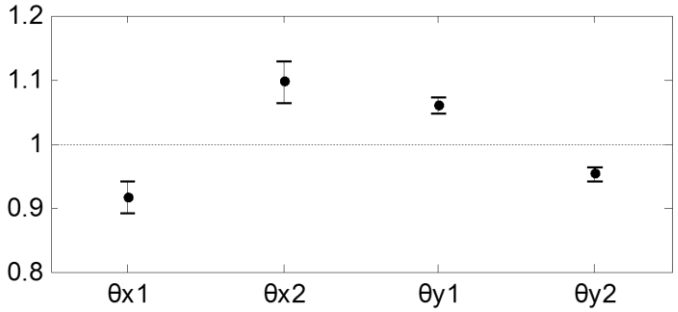

Figure 6 Identified stiffness parameters in Stage II, one-storied building, with alignment error

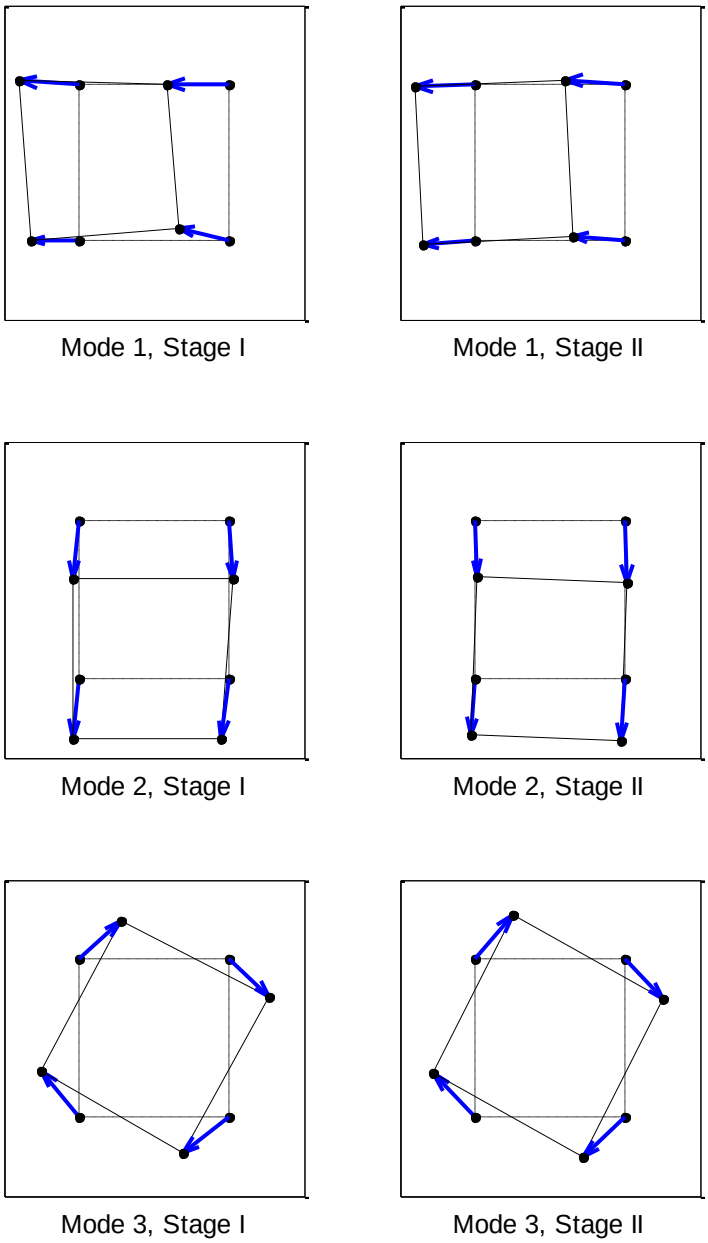

Figure 7 Comparison of mode shapes, one-storied building with alignment error. Left – MPV identified in Stage I; Right – resulting from the most probable structural model in Stage II

(a)

(b)

Figure 8 Laboratory model. (a) Overview; (b) Hole in the front left column on the first floor.

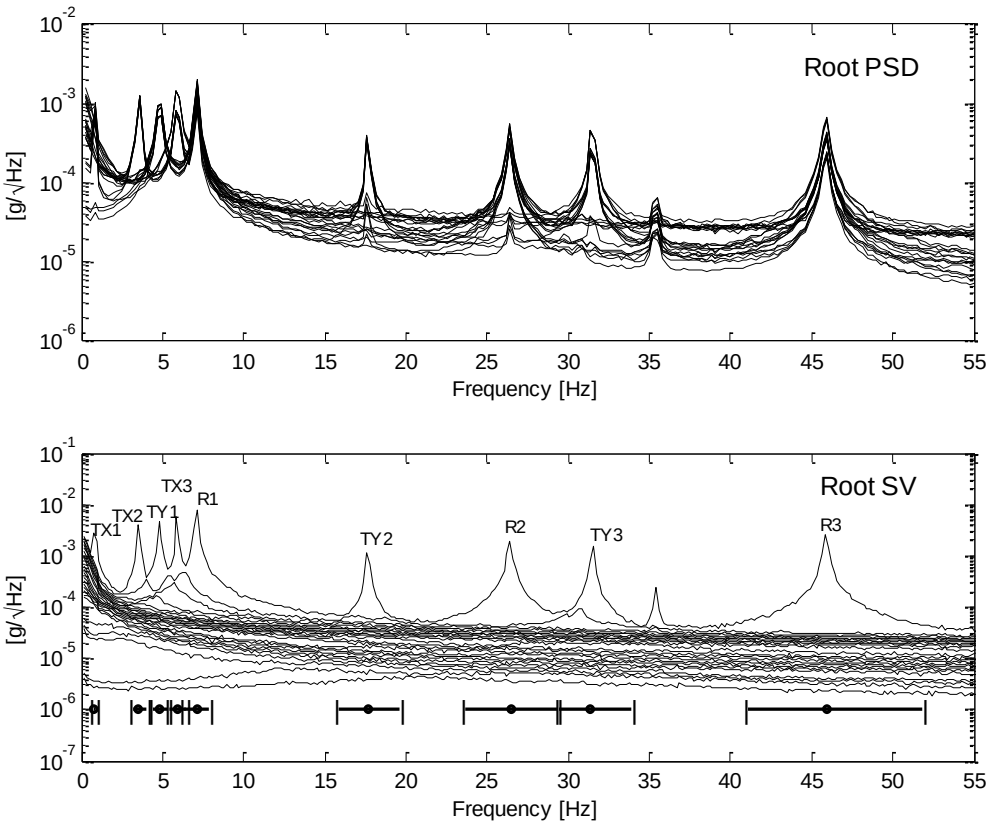

Figure 9 Root PSD and root SV spectra, laboratory frame

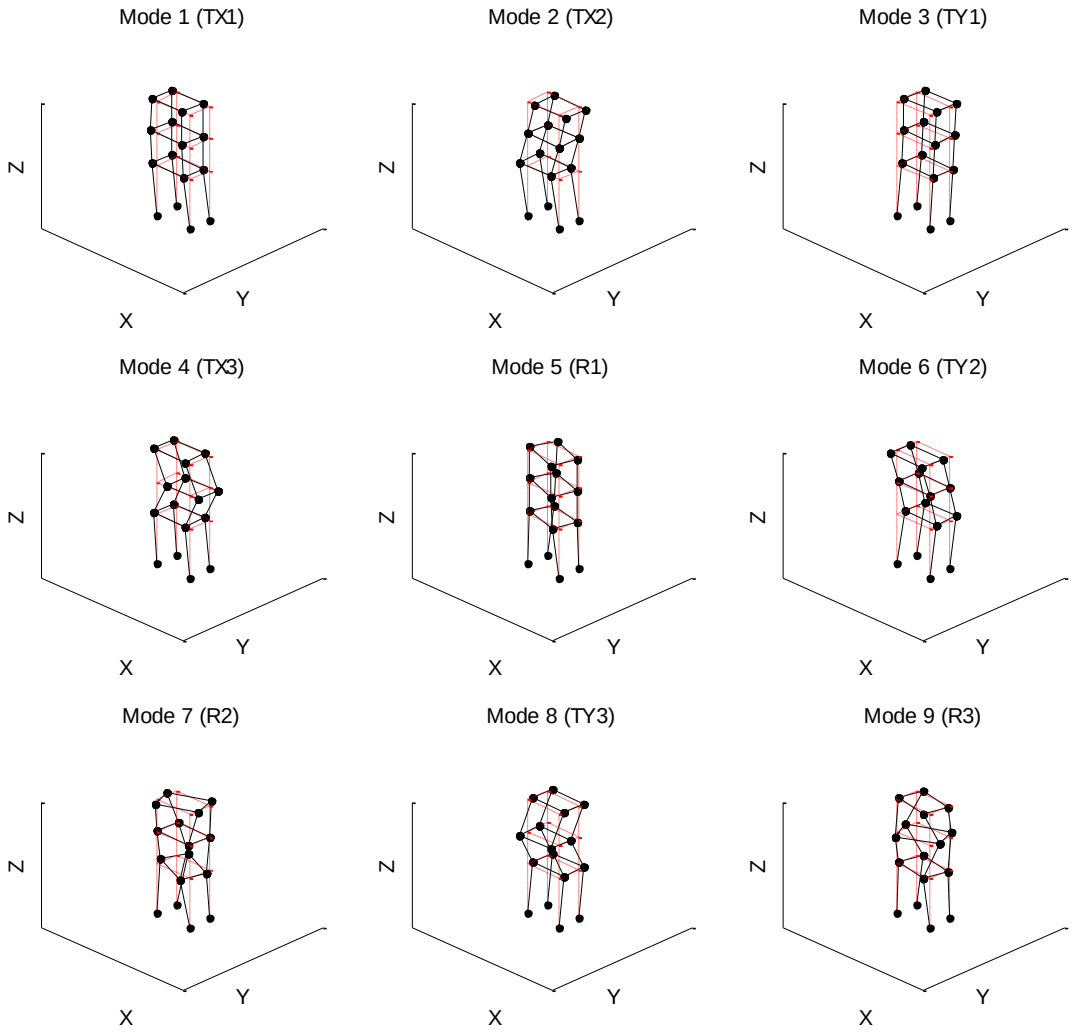

Figure 10 Most probable mode shapes, laboratory frame

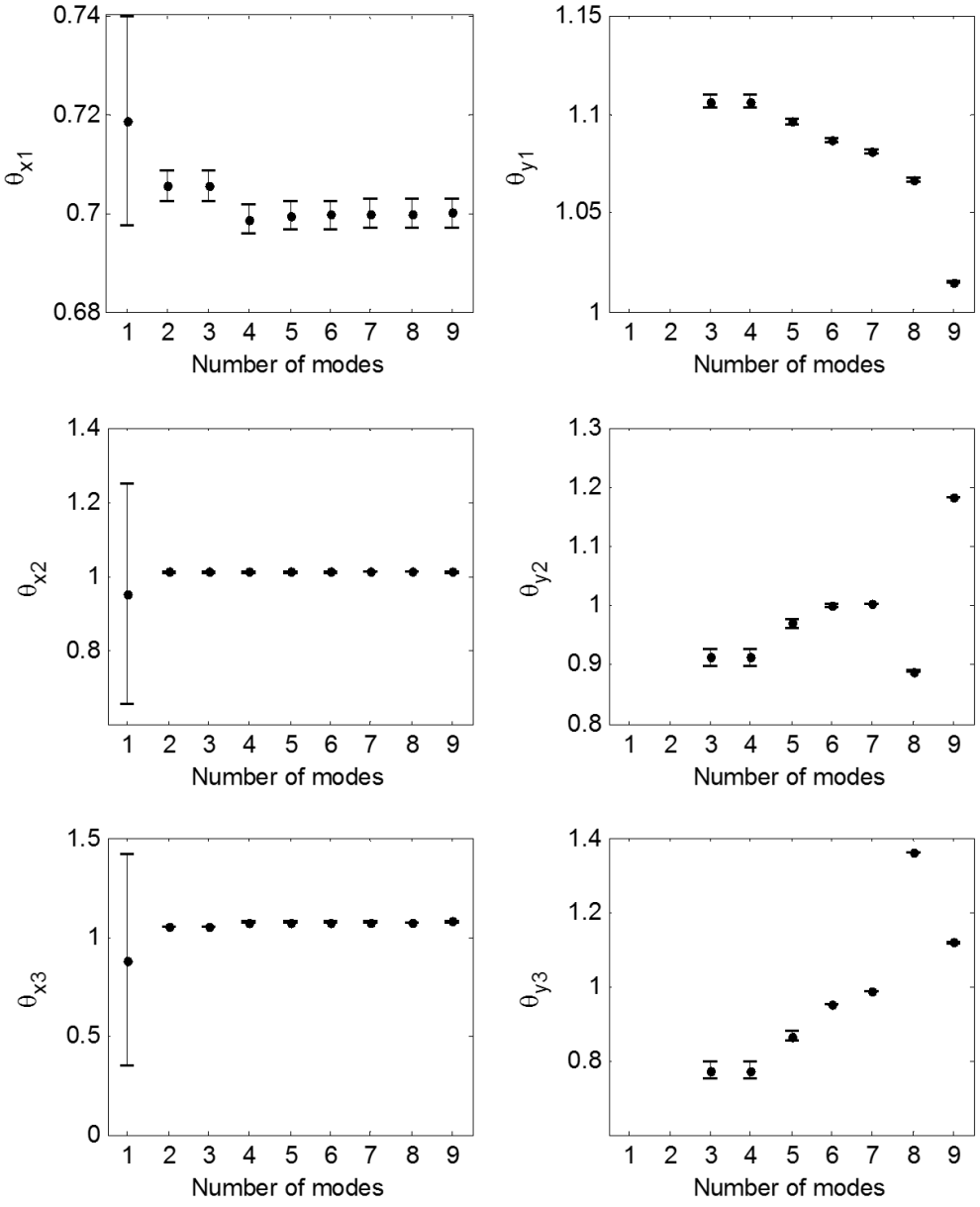

Figure 11 Identified stiffness parameters (MPV and +/- 2 standard deviations) based on different number of modes

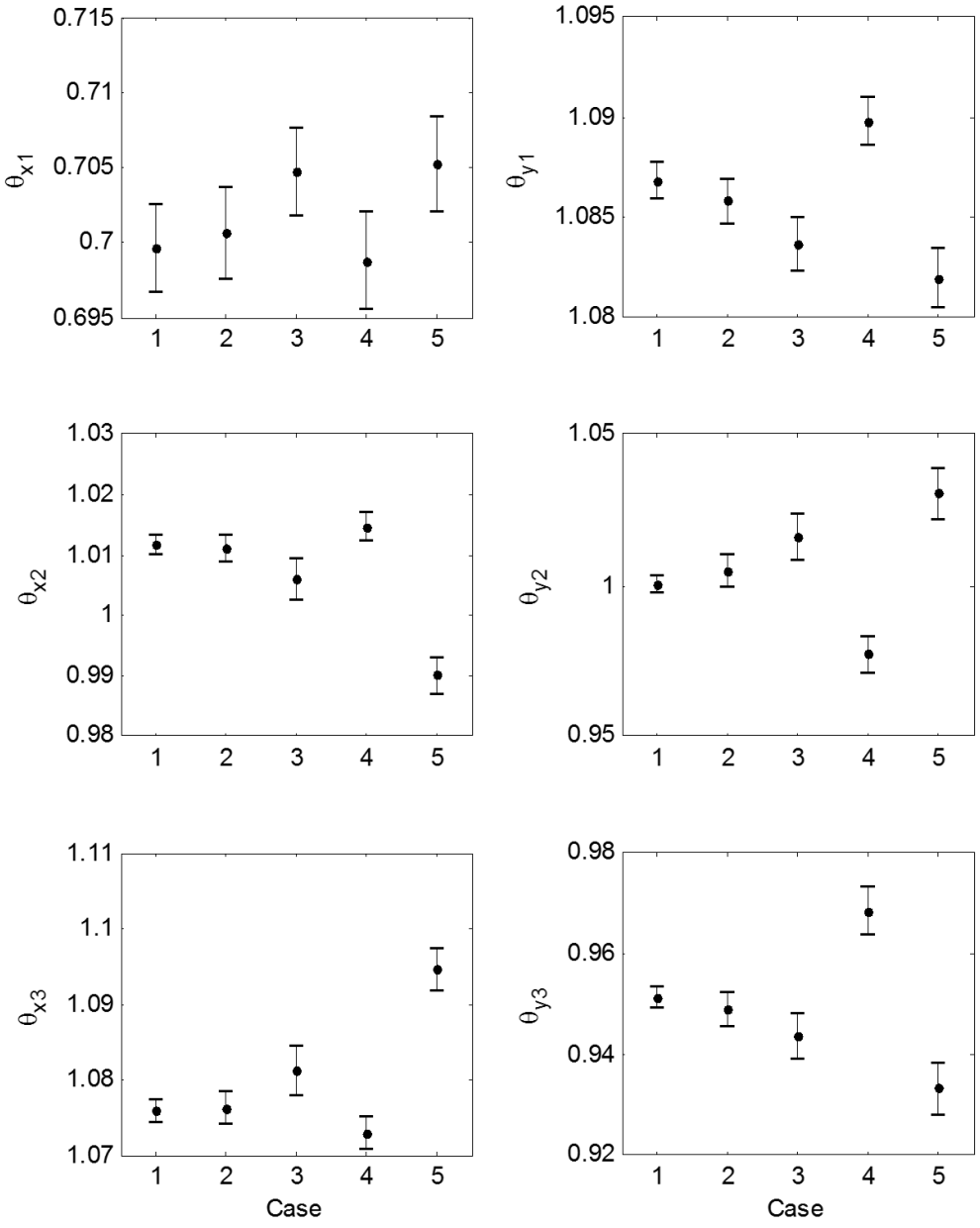

Figure 12 Identified stiffness parameters (MPV and +/- 2 standard deviations) based on different measured dofs, including the first six modes. Case 1: four columns, 1-3/F; Case 2: two columns on the left, 1-3/F; Case 3: two columns on the left, 1/F & 2/F; Case 4: two columns on the left, 1/F & 3/F; Case 5: two columns on the left, 2/F & 3/F.